# Daily flow simulation in Thailand Part II
# Unraveling effects of reservoir operation

Wannasin, C.; Brauer, C. C.; Uijlenhoet, R.; van Verseveld, W. J.; Weerts, A. H.

# Daily flow simulation in Thailand Part II: Unraveling effects of reservoir operation

C. Wannasin [a,*], C.C. Brauer [a], R. Uijlenhoet [a,b], W.J. van Verseveld [c], A.H. Weerts [a,d]

[a] Hydrology and Quantitative Water Management Group, Wageningen University and Research, P.O. Box 47, 6700AA Wageningen, The Netherlands
[b] Department of Water Management, Faculty of Civil Engineering and Geosciences, Delft University of Technology, P.O. Box 5048, 2600GA Delft, The Netherlands
[c] Catchment and Urban Hydrology, Department of Inland Water Systems, Deltares, P.O. Box 177, 2600MH Delft, The Netherlands
[d] Operational Water Management, Department of Inland Water Systems, Deltares, P.O. Box 177, 2600MH Delft, The Netherlands

ARTICLE INFO

ABSTRACT

Study region: Upper region of the Greater Chao Phraya River (GCPR) basin in Thailand.
Study focus: The upper GCPR basin is highly regulated by multipurpose reservoirs, which obviously have altered the natural streamflow. Understanding quantitative effects of such alteration is crucial for effective water resource management. Therefore, this study aims to assess how reservoir operation affects the water balance, daily flow regime and extreme flows in this basin. For this purpose, we reconstructed streamflow in the naturalized (no reservoir) and baseline operation scenarios using the (~1 km resolution) distributed model. To overcome data scarcity, we ran the model with global data and parameterization. A target storage-and-release-based reservoir operation module was applied in the baseline operation scenario. The model results were analyzed in comparison to observations in a wet year, a dry year, and the period 1989–2014.
New hydrological insights for the region: The reservoir operation resulted in more evaporation. It inverted the natural flow seasonality and smoothed the daily flow regime with decreasing high flows, increasing mean flows and low flows, greater baseflow contribution, and lower flashiness. It prevented or mitigated many historical extreme flow incidents. The annual flood peaks and minimum flows were markedly mitigated in terms of both magnitudes and frequencies, but their timing became more variable and difficult to predict. Altogether, the results highlighted the importance of effective decision making for real-time operation, which remain challenging in practice.

## 1. Introduction

The majority of rivers around the world are fragmented by dammed reservoirs (Zhou et al., 2016). Although several dams have been removed at the end of their useful lives, they are outnumbered by those in operation and under construction (O'Connor et al., 2015). The current boom in dammed reservoir construction takes place particularly in regions with emerging economies like Southeast Asia (SEA), where it serves not only for irrigation and hydrological hazard control, but also for hydropower generation (Zarfl et al., 2015). In fact, SEA has recently become the region with the highest investment for large multipurpose reservoirs (Siciliano et al., 2015). Currently, there are more than 130 new projects of large reservoirs planned in Laos, Malaysia, Cambodia, Myanmar and at the

* Corresponding author.
  E-mail address: chanoknun.wannasin@wur.nl (C. Wannasin).

border of Myanmar-Thailand (Siciliano et al., 2015). Therefore, it is undeniable that dammed reservoirs are a necessity for water resource management and play an important role in flood and drought mitigation in SEA.

Despite their benefits, dammed reservoirs remain controversial due to their potentially negative impacts on streamflow, environment and society. Reservoir operations alter the natural flow regime, i.e., flow rate, flow magnitude and fluctuation, in particular the duration, timing and frequency of wet and dry extremes, from the daily to the long-term scale (Graf, 2006; Mittal et al., 2016; Li et al., 2017). On the one hand, reservoir operations can attenuate flood and drought events by smoothing streamflow, with lower flood peaks and higher baseflows (e.g., Lee et al., 2017; Wu et al., 2018; Gai et al., 2019). On the other hand, hydrological extremes can be intensified by ineffective management of reservoir water, which in some cases had greater influence than climate change (e.g., Graf, 2006; Mittal et al., 2016; He et al., 2017; Di Baldassarre et al., 2018). Since SEA has an increasing number of dammed reservoirs while being highly exposed to hydrological hazards (Trenberth et al., 2014; Arnell and Gosling, 2016), there is an urgent need to evaluate effects of reservoir operations on streamflow in specific contexts of this region.

The Greater Chao Phraya River (GCPR) basin in Thailand is one of the most highly regulated river basins by dammed reservoirs in SEA. The delta area in the basin is also among the most vulnerable areas in the region (Yusuf and Francisco, 2009). Despite water resource management with several multipurpose reservoirs, the GCPR basin still suffers from floods and droughts regularly, which devastate the agricultural and environmental resources, and subsequently the economic development of the country and the region (Takeda et al., 2016; Kinouchi et al., 2018). While most reservoirs in neighboring basins, such as in the Mekong River, have been constructed in recent years (Urban et al., 2018), the main reservoirs in the GCPR basin have been operated for over half a century and data on daily reservoir outflows are available for the last 25 years. The longer period of observational records in the GCPR basin allows for a comprehensive analysis. Therefore, investigating effects of reservoir operations on streamflow in this basin can also contribute to the understanding and improvement of water resource planning and management in other basins in SEA.

Previous studies mentioned conflicting causes of hydrological hazards in the GCPR basin. Komori et al. (2012) suggested that the 2011 GCPR flood, one the most catastrophic floods ever recorded in SEA, was driven by intense precipitation, in line with the finding of Sayama et al. (2015) that a 1% increase in precipitation caused a 4.2% increase in flood inundation in the basin. Meanwhile, Van Oldenborgh et al. (2012) concluded that the 2011 GCPR flood volumes were magnified by non-meteorological factors, particularly reservoir water management. The study of Gale and Saunders (2013) supported this statement as they found that the precipitation anomaly was higher in 1995 than in 2011, but the 1995 flood was not nearly as severe as the 2011 flood. However, considering the limited number of studies, the respective roles of reservoir operations and extreme weather on hydrological hazards in the GCPR basin remain unclear.

The attention to reservoir operations and their effects on streamflow in the GCPR basin was drawn after the 2011 flood. Komori et al. (2012) provided an overview of reservoir water management in 2011. The spectrum analysis by Tebakari et al. (2012) indicated that the observed streamflow downstream of the reservoirs had a periodicity of seven days due to the irrigation purpose. Since daily streamflow data for this basin have been available only after the reservoir constructions, it is impossible to identify changes and trends of observed streamflow from natural to regulated conditions. Therefore, several studies took the approach of comparing observed streamflow to naturalized (without reservoir) streamflow obtained from hydrological models (Komori et al., 2013; Wichakul et al., 2013; Hanasaki et al., 2014; Mateo et al., 2014; Sayama et al., 2015). All these studies highlighted effects of reservoir operations on downstream flows in the GCPR basin by analysing hydrographs. However, they mainly focused on reservoir effects on high flows, particularly during the 2011 flood events, and excluded reservoir effects on low flows. Most studies assessed reservoir effects on hydrographs in the downstream floodplain, which may be influenced by effects of intensive irrigation. In addition, reservoir effects on the water balance and daily flow regime in the GCPR basin have not been investigated.

Understanding the naturalized water balance and daily flow regime, and how they have been modified by reservoir operations is essential not only from a hydrological viewpoint, but also from socio-economic and environmental perspectives. The knowledge assists dam operators and water resource managers in planning and developing strategies to optimize both human consumption and ecosystem maintenance. It also supports adaptive management strategies to predict and deal with such probable changes for other existing or planned reservoirs in the same or a neighboring basin. Moreover, it helps to prepare for expected changes in streamflow after dam removals in the future. However, the main challenge in investigating the naturalized water balance and daily flow regime in many river basins, including the GCPR basin, is the lack of observed streamflow data prior to reservoir constructions.

One of the approaches to overcome the lack of observed streamflow data in reservoir operation studies is hydrological modeling. Many hydrological models can represent reservoir operation schemes and hydrological responses as part of rainfall-runoff processes (e. g., Zajac et al., 2017; Canuto et al., 2019; Gai et al., 2019). Distributed hydrological models are often used for reservoir system modeling because they allow the calculation of water interactions between a reservoir and its surrounding area in a spatially distributed manner. However, distributed models usually require an enormous amount of data, which is a drawback for data-scarce areas like in SEA. In addition, distributed models usually require area-specific and scenario-specific calibration, which poses a high risk of overparameterization and long computation times.

To tackle these issues, we used the (~1 km resolution) distributed wflow_sbm model with global data and parameterization (Schellekens et al., 2019; Imhoff et al., 2020). The model has been set up and evaluated for the upper region of the GCPR basin, as elaborated in a companion paper (Wannasin et al., 2021). With a target storage-and-release-based reservoir operation module (ROM), the model was applied to simulate daily streamflow in the baseline operation scenario, when reservoir releases were determined solely based on generalized operation rules without real-time control. In this study, we further apply the model to simulate daily streamflow in the naturalized scenario. By comparing the simulation results in the naturalized and baseline operation scenarios to the observations, which represent the real-time operation, we can comprehensively analyze effects of reservoir operations, in terms of generalized operation rules and real-time control, on daily streamflow.

The main aims of this study are to (i) quantify effects of reservoir operations on the water balance and daily flow regime and (ii) distinguish effects of reservoir operation and extreme weather on extreme flows in the GCPR basin. We analyzed the simulated and observed streamflows over a 25-year period of 1989–2013. By focusing on streamflow at the dam locations instead of floodplain gauges, we excluded probable influences of downstream irrigation and highlighted the effects of reservoir operations alone.

The paper is organized as follows. In Section 2, we describe the study area. In Section 3, we summarize the model application and required data. Next, our analysis methods are presented in Section 4, including the evaluation of naturalized flow simulations (Section 4.1), the evaluation of reservoir effects on the water balance (Section 4.2), the evaluation of reservoir effects on daily flow regime (Section 4.3) and the evaluation of effects of reservoir operations and extreme weather on extreme flows (Section 4.4). We present the results in Section 5 and the discussion in Section 6, followed by the conclusion and outlook in Section 7.

## 2. Study area

The Greater Chao Phraya River basin (GCPR), located in the heart of Thailand, covers approximately 158,600 km$^2$ (30%) of the country's area (Fig. 1). It is divided into the upper and lower regions at Nakhon Sawan valley where the upstream rivers, Ping, Wang, Yom and Nan, join and form the Chao Phraya, which drains into the Gulf of Thailand. Since the main goal of this study is to assess the reservoir effects, we focused on the upper region (~104,000 km$^2$), where the main reservoirs are located. Its major areas are covered by forests and grasslands, which have been gradually replaced by agricultural areas, particularity rice fields (Jamrussri and Toda, 2017).

The climate of the upper GCPR basin is distinctly divided into the wet (rainy) and dry seasons, which are influenced by monsoons and tropical cyclones. Considering the seasonality, the Thai water-year starts from April 1$^{st}$ of any given year to March 31$^{st}$ of the following year (i.e., the year 2011 is from April 1$^{st}$, 2011 to March 31$^{st}$, 2012). The water-year and water-yearly hereafter will be referred to as year and yearly/annual.

There are seven multipurpose reservoirs in the upper GCPR basin, serving irrigation water supply, hydroelectricity generation and flood control. The Bhumibol reservoir (storage capacity 13.46 billion m$^3$) has been operated on the Ping River since 1964 and the Sirikit reservoir (storage capacity 9.51 billion m$^3$) has been operated on the Nan River since 1977 (reservoir locations shown in Fig. 1). Another five reservoirs were constructed on the Ping River (two), Wang River (two) and Nan River (one). A plan to build the first
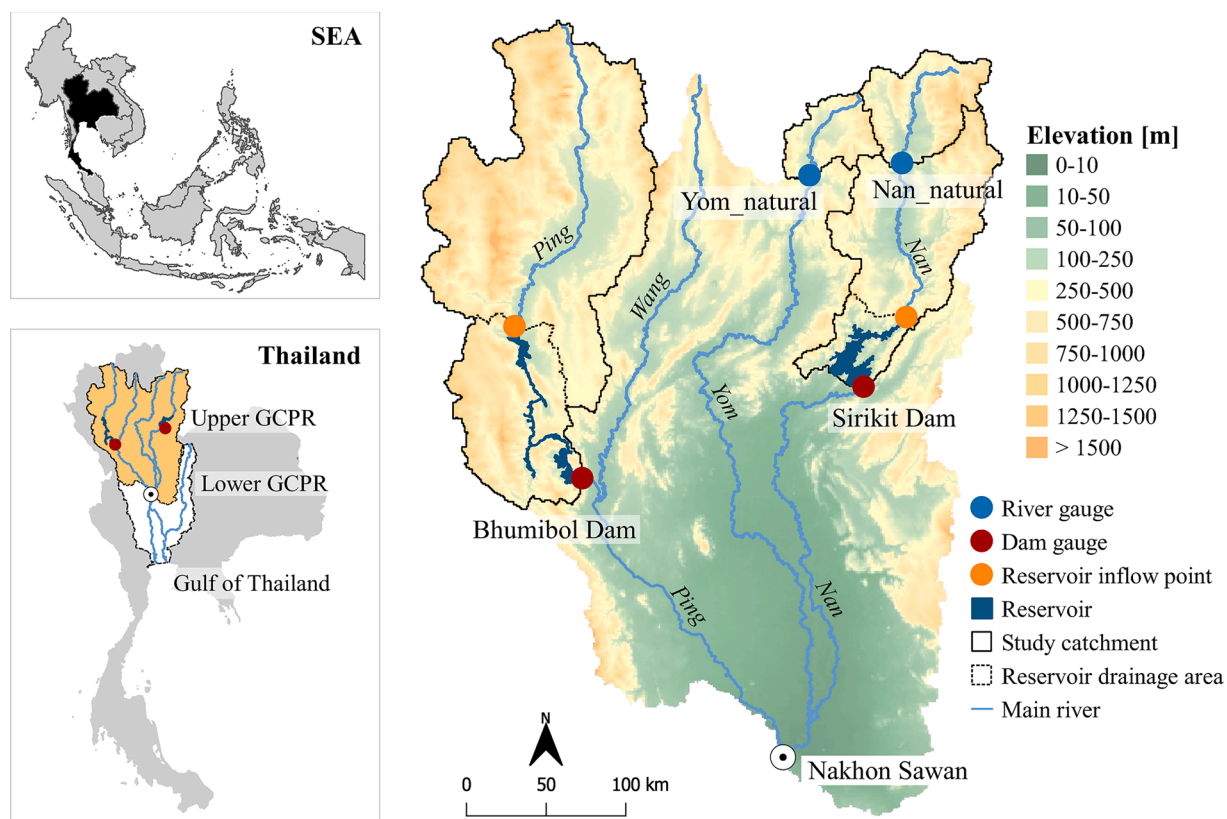


**Fig. 1.** Overview of the study area. The top left panel shows the location of Thailand in Southeast Asia, the bottom left panel shows the location of the GCPR basin in Thailand, and the right panel shows the spatial distribution of reservoirs and study catchments in the upper GCPR basin (from Wannasin et al. (2021). In the right panel, the solid lines indicate the catchment boundaries from the headwater until the gauge location, while the dash lines indicate the drainage areas from the inflow point of each reservoir to the dam location.

reservoir on the Yom River has been postponed since 1980 due to controversial discussion about the myriad of negative environmental and social impacts (Apichitchat and Jung, 2015). Since the five reservoirs, of which four are located upstream of the Bhumibol reservoir, only account for 7% of the total reservoir capacity in the upper region, we assumed that their effects on downstream flows are insignificant at the basin scale and thus focused on the two major reservoirs, Sirikit and Bhumibol. The GCPR basin endures regular occurrences of floods and droughts. In rainy seasons, flooding often occurs because the downstream part of the upper region and most of the lower region are gently sloped. Hence, high discharge from the upper region is likely to flood the lower region. In many occasions, upstream floodwater cannot flow down at once due to the elevated water level in the Chao Phraya River itself. As a consequence, the floodplain above the narrow section at Nakhon Sawan is inundated for a long period (Sayama et al., 2015). In dry seasons, droughts tend to occur when the water storage in the major reservoirs fails to meet the irrigation and consumption demands, e.g., the Bhumibol water shortage in 2016 (Zenkoji et al., 2019). The water shortage leads to large losses in agricultural and industrial production (Kinouchi et al., 2018). Therefore, it is imperative to understand reservoir operations and their effects on the water balance and flow regime in the upper region in order to enhance their capabilities to mitigate hydrological extremes for the entire basin.

In this study, we analyzed the water balance and streamflow in two regulated catchments, the Sirikit and Bhumibol catchments. The drainage areas from the headwater until the dam location are 13,155 km$^2$ for Sirikit and 25,988 km$^2$ for Bhumibol. However, we defined the Sirikit catchment (2020 km$^2$ and the Bhumibol catchment (6863 km$^2$) as the drainage areas from the inflow point of each reservoir in the hydrological model to the dam location (see Fig. 1) to be able to analyze their upstream inflows in the water balance. Two natural catchments located upstream of the reservoirs, the Nan_natural (3546 km$^2$) and Yom_natural (2018 km$^2$), were also investigated. They were used to point out the resemblance of the upstream natural streamflow to the naturalized flow simulation of the Sirikit and Bhumibol catchments since the observations prior to the reservoir construction are unavailable for the model result validation. Locations of the four catchments are shown in Fig. 1. By focusing on the reservoir catchments instead of floodplain catchments downstream, we avoided effects of intensive irrigation.

## 3. Model and data

The application of the wflow_sbm model with the simplified target storage-and-release-based reservoir operation module (ROM) in this study is summarized below. The full description of wflow_sbm is provided in Schellekens et al. (2019) and the ROM calculation is explained in Wannasin et al. (2021). Details on the model development and evaluation for the upper GCPR basin can be found in Wannasin et al. (2021).

The wflow simple bucket model, so-called wflow_sbm, is a distributed hydrological model in the wflow modeling platform built within the PCRaster and python environments (Schellekens et al., 2019). It was developed based on the Topog SBM model (Vertessy and Elsenbeer, 1999) and has shown good performance in the applications in many basins around the world (e.g., López López et al., 2016; Hassaballah et al., 2017; Giardino et al., 2018; López López, 2018; Gebremicael et al., 2019; Imhoff et al., 2020). For the entire upper GCPR basin, the model has been set up at the ~1 km spatial resolution and the 3-hourly timescale (Wannasin et al., 2021). In this study, the simulation of the wflow_sbm model with the ROM for the Sirikit and Bhumibol reservoirs is referred to as the baseline operation scenario, while the simulation without the reservoir existence is referred to as the naturalized scenario.

To overcome data scarcity in the upper GCPR basin, which is a common challenge in SEA, most required spatial data for wflow_sbm were obtained from global databases. The geospatial data included the elevation map from the Shuttle Radar Topography Mission (SRTM; Jarvis et al., 2008), the land cover map from GLOBCOVER (Bontemps et al., 2011), the soil map from SoilGrids (Hengl et al., 2017) and the river network map from the Royal Irrigation Department of Thailand (RID). The meteorological data comprised precipitation (*P*) from the Multi-Source Weighted-Ensemble Precipitation Version 2 database (MSWEP V2; Beck et al., 2019) and potential evapotranspiration (*PET*) from the eartH2Observe database (Schellekens et al., 2017). The hydrological data consisted of observed daily streamflow, observed daily reservoir storage and reservoir operating rule curves of each reservoirs provided by RID and the Electricity Generating Authority of Thailand (EGAT). Only the river network and observed hydrological data were derived from local sources.

As for the wflow_sbm model parameterization, seamless distributed parameter maps was implemented instead of full calibration, which prevented overparameterization and reduced computation times (Wannasin et al., 2021). The soil-related parameter maps (e.g., hydraulic conductivity) were calculated with the Brakensiek pedotransfer function (Brakensiek et al., 1984) and are not subject to change from the naturalized scenario to the regulated scenario. Only one soil-related parameter, *KsatHorFrac*, which is the factor for calculating horizontal saturated conductivity and thus greatly affects the lateral subsurface flow, was manually calibrated (Wannasin et al., 2021). The land cover-related parameter maps were obtained from global databases (e.g., leaf-area index) or by assigning parameter values from literature review (e.g., Manning's roughness coefficient) to the GLOBCOVER land cover types. To create the land cover-related parameter maps for the naturalized scenarios, we firstly converted GLOBCOVER grid cells marked as reservoir water to naturalized land cover types using the nearest-neighbor-upscaled interpolation method. Then, we assigned parameter values for the new land cover types. We assumed that impacts of gradual land use changes, such as agricultural expansion and urbanization, were much smaller at the basin scale compared to impacts of reservoirs. Therefore, the uncertainty of naturalized land cover and thus the uncertainty of naturalized parameters were assumed negligible.

In the baseline operation scenario, the number of generalized operational and physical parameters of the ROM were minimized to overcome the data scarcity. The parameter values were determined based on the reported operating rule curves and databases provided by RID and EGAT and were applied without calibration, as elaborated in Wannasin et al. (2021).

## 4. Evaluation methods

We carried out the 25-year simulation from 1989 to 2013 according to the naturalized scenario (wflow_sbm without reservoir; sim_nat) and baseline operation scenario (wflow_sbm with the ROM; sim_base). The daily simulation results were then analyzed in comparison to the daily observations, which reflect the real-time operation. We used 2006 as the representative year for wet conditions and 2013 for dry conditions. Although these two years were not the most extreme years recorded, they were carefully chosen to distinguish effects of reservoir operations and extreme weather on extreme flows.

By focusing on the selected catchments (locations shown in Fig. 1), we conduct the analyses in four parts. Firstly, we validated the simulated streamflows in the naturalized scenario. Secondly, we used the data from the naturalized scenario, baseline operation scenario, and observations to quantify effects of reservoir operations on the long-term water balance components. Next, we assessed reservoir effects on key signatures of the daily flow regime. Lastly, we examined effects of reservoir operations and extreme weather on the frequency and recurrence of extreme flows.

### 4.1. Simulated streamflow evaluation

Since the daily streamflow observations prior to the construction of the Sirikit and Bhumibol reservoirs are unavailable, it was impossible to directly evaluate the accuracy of the naturalized flow simulation for the Sirikit and Bhumibol catchments. Therefore, we validated their naturalized flows by visually comparing the resemblance of their daily hydrographs to those of the natural catchments upstream. Note that the model performance in the baseline operation scenario has been evaluated in Wannasin et al. (2021).

### 4.2. Analyses of reservoir effects on the water balance

To evaluate effects of reservoir operations on the catchment water balance, the water balances of the upstream natural catchments were deliberated as baselines. We then compared water balance components of the regulated catchments among the naturalized scenario, baseline operation scenario and observations. Precipitation ($P$) and upstream inflow ($I$) are partitioned into actual evapotranspiration ($AET$), streamflow ($Q$) and storage change ($\Delta S$, which includes both subsurface storage and reservoir storage) during a given time period. Since some water balance components (e.g., groundwater storage change and seepage) are difficult to estimate, they are often determined as the residuals of the water balance equation (Kampf and Burges, 2010). The water balance is expressed as

$$P + I - AET - Q = \Delta S, \tag{1}$$

where $I$ and $Q$ refer to streamflow in this context. Subsurface and overland flows across the catchment boundary were excluded as they were negligible in the simulations and unavailable from the observations. In the naturalized and baseline operation scenarios, the water balance components on the left-hand side of Equation (1) were extracted from the wflow_sbm simulations. Then, $\Delta S$ was calculated as the residual of the water balance. For comparison, we also calculated $\Delta S$ using observed $Q$ and made use of MSWEP V2 $P$, and $I$ and $AET$ data from the simulations due to unavailable observed data.

### 4.3. Analyses of reservoir effects on the daily flow regime

To understand effects of reservoir operations on the daily flow regime, we focus on the Sirikit reservoir and analyzed three streamflow signatures: the flow-duration curve (FDC), baseflow index (BFI) and flashiness index (FI). The signatures were compared among the naturalized scenario, baseline operation scenario and observation. Considering the missing data in the observed streamflow record, we quantified the signatures for each year available and for the long periods of 1989–1997 and 2003–2013.

#### 4.3.1. Flow-duration curve

The daily flow regime can be summarized in the comprehensive form of the FDC, which is the empirical cumulative frequency of daily streamflow as a function of the percentage of time that the streamflow is exceeded. The slope of the FDC represents the streamflow variability, including both high and low flows. To quantify reservoir effects on the daily FDC, we calculated and compared the slopes of the FDCs, median flows ($Q_{50}$), high flows and low flows among the simulations and observation. We defined high flows as the flows that are exceeded 10% of the time ($Q_{10}$), and low flows as being exceeded 90% of the time ($Q_{90}$). As generally the FDC between the 33$^{rd}$ and 66$^{th}$ flow percentiles is nearly linear on a semi-log scale (Sawicz et al., 2011), the FDC slope (Slope$_{FDC}$) is defined as

$$\text{Slope}_{FDC} = \frac{ln(Q_{33}) - ln(Q_{66})}{0.66 - 0.33}, \tag{2}$$

where $Q_{33}$ and $Q_{66}$ are the daily streamflow values at the 33$^{rd}$ and 66$^{th}$ percentile. A steeper slope refers to higher variability of daily flows.

#### 4.3.2. Baseflow index

Baseflow is part of streamflow that comes from persistent, delayed sources and is thus highly correlated to the water storage in a catchment (Hisdal et al., 2004). In natural catchments, baseflow mainly comes from groundwater, whereas in catchments with highly

regulated dammed reservoirs, baseflow mainly comes from reservoir water. In this study, we separated baseflow from the daily streamflow time series using the separation procedure of Gustard et al. (1992). We calculated the minima of 5-day non-overlapping consecutive periods and identified turning points of the minima sequence. A minimum became a turning point if 0.9 times its value was less than or equal to the neighboring minimum. Connecting the turning points formed the baseflow separation line in the hydrograph. Daily baseflow values were then assigned with linear interpolation between the turning points. The baseflow was set equal to the total streamflow on any day that the estimated baseflow exceeded the total streamflow.

The base flow index, BFI [–], is the ratio of baseflow to total streamflow in a given period,

$$\text{BFI} = \frac{\sum_{i=1}^{n} Q_{\text{base}}}{\sum_{i=1}^{n} Q_{\text{total}}}, \tag{3}$$

where $Q_{\text{base}}$ refers to the daily baseflow and $Q_{\text{total}}$ refers to the daily streamflow, $i$ is the given time step (day) and $n$ is the number of days in the given period. BFI values range between 0 and 1. A higher index value means a higher contribution of baseflow to total streamflow. To quantify reservoir effects on the daily baseflow, we calculated and compared the BFI values among the simulated and observed streamflow time series.

### 4.3.3. Flashiness index

While the Slope$_{\text{FDC}}$ indicates the overall variability of daily streamflow regardless of the chronological order, flashiness reflects the absolute day-to-day fluctuations in the streamflow magnitude. Flashy streams have much daily change, while stable streams have little daily change (Poff et al., 1997). We used the Richards-Baker flashiness index (FI [–]; Baker et al., 2004), which is quantified by the ratio of daily streamflow fluctuations relative to the total streamflow in a given period,

$$\text{FI} = \frac{\sum_{i=1}^{n} |Q_i - Q_{i-1}|}{\sum_{i=1}^{n} Q_i}, \tag{4}$$

where $Q$ is daily streamflow, $i$ is the given time step (day) and $n$ is the number of days in the given period. FI values range between 0 and 2, of which zero represents an absolutely constant flow; higher index values mean larger fluctuations of daily streamflow. Streamflow time series with a steep Slope$_{\text{FDC}}$ tend to give a high FI value. However, streamflow time series with similar Slope$_{\text{FDC}}$ values can result in very different FI values because FI excludes the seasonal and inter-annual variability within the given period. Therefore, to quantify reservoir effects on the daily flashiness, we calculated and compared the FI values among the simulated and observed streamflow time series.

### 4.4. Analyses of reservoir and extreme weather effects on extreme flows

To understand effects of reservoir operations on extreme flows, we focus on the Sirikit reservoir and assessed the frequency and recurrence of extreme flows in relation to magnitude and timing among the simulations and observation. In this study, extreme flows refer to annual maximum daily flows (*AMAX*) and annual minimum daily flows (*AMIN*). For the upper GCPR basin, very high flows in
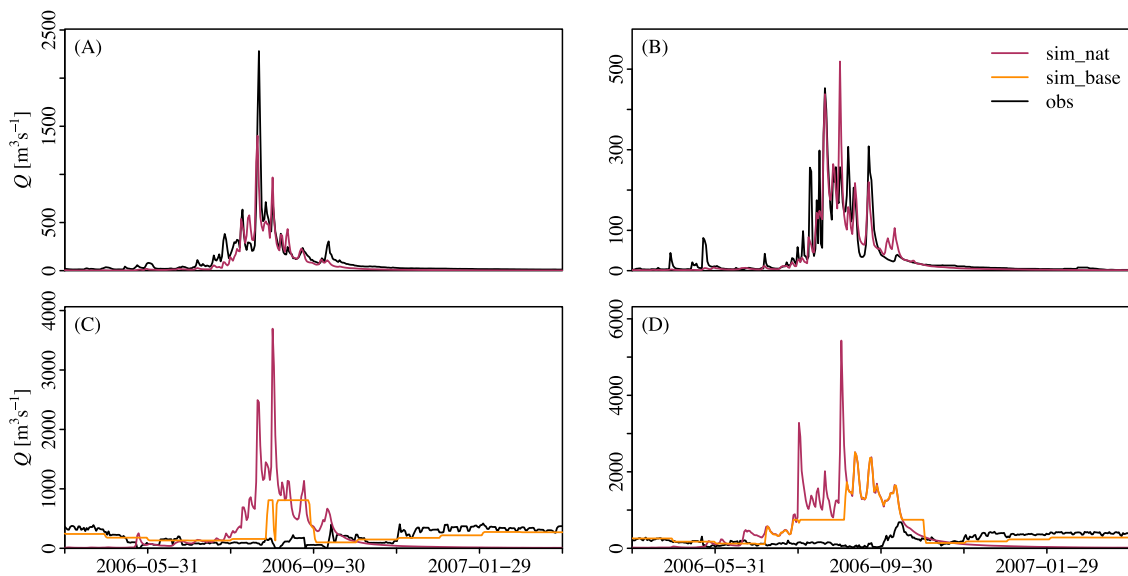


**Fig. 2.** Simulated and observed daily streamflows for the Nan_natural (A), Yom_natural (B), Sirikit (C) and Bhumibol (D) catchments in the wet year (2006). The streamflow in the naturalized scenario (sim_nat) is shown in red lines, the baseline operation scenario (sim_base) in orange lines and the observations (obs) in black lines. Since the hydrographs in the dry year (2013) show similar flow patterns, they are not included here.

the dry season are usually employed for irrigation and do not cause flooding. Likewise, very low flows in the rainy season are meant to prevent downstream inundation and do not lead to drought. Therefore, we computed *AMAX* in the period of May–October (rainy season) and *AMIN* in the rest of the year. Although Durrans (1988) suggested that total probability methods are suitable for estimating flood frequency in regulated catchments, the capability of the Gumbel extreme value distribution to represent flood frequency in reservoir-dominated catchments has been demonstrated (e.g., Batalla et al., 2004; Lee et al., 2017). In addition, the Gumbel distribution was suggested as one of the best-fit functions to analyze yearly low flows (Matalas, 1963; Langat et al., 2019). Therefore, it was selected for the frequency analysis of *AMAX* and *AMIN* based on the 25-year period of daily streamflow data in this study.

To distinguish effects of extreme weather on daily extreme flows, we assessed the relationship between the *AMAX* or *AMIN* and the associated weather. We used the sum of precipitation and upstream inflow minus actual evapotranspiration ($P + I - AET$), here called effective inflow, on the day that the *AMAX* or *AMIN* occurred and over the 30 days preceding the extreme flow event to represent the weather condition.

## 5. Results

### 5.1. Naturalized flow

The visual comparison of the simulated daily streamflow in the naturalized scenario (sim_nat), $Q_{sim\_nat}$, for the Sirikit and Bhumibol catchments to the daily streamflow observations (obs), $Q_{obs}$, for the upstream natural catchments implies satisfactory results produced by the wflow_sbm model. The daily hydrographs of $Q_{sim\_nat}$ for both regulated catchments, shown as red lines in Fig. 2(C) and (D), present trends comparable to the hydrographs for the upstream natural catchments in Fig. 2(A) and (B). The strong seasonal variation, with very low flows in the dry season as well as steep rising limbs and high flood peaks in the rainy season, suggests that the wflow_sbm model can reconstruct the naturalized flows regardless of the uncertainty in the naturalized land cover setting.

### 5.2. Effects of reservoir operation on the water balance

The simulated water balances of the Nan_natural and Yom_natural catchments are similar to each other in terms of water budget distribution based on the yearly average data (Table 1). Note that these natural catchments are located at the headwaters and thus do not have upstream inflows (see their locations in Fig. 1). The annual *AET/PET* ratios for the two catchments ranged between 0.68 and 0.70. Approximately two-thirds of the annual *P* evaporated and one-third flowed downstream. The annual $Q_{sim\_nat}$ tends to underestimate the annual $Q_{obs}$, especially for the Nan_natural catchment. Consequently, the disparity between the simulated and observed storage changes ($\Delta S_{sim\_nat}$ and $\Delta S_{obs}$) is also considerable. However, it should be noted that the $\Delta S_{obs}$ values were calculated using the MSWEP V2 *P* data and the simulated *AET* data from the naturalized scenario since the observed *AET* data are unavailable. These data sources could also be a source of bias, affecting the simulated storage.

The simulated water balance in the baseline operation scenario (sim_base) of the Sirikit catchment is different from its naturalized scenario (Table 1). Note that the Sirikit catchment is located midstream and thus receives inflows from upstream (see its location in Fig. 1). The annual *AET/PET* ratio increased from 0.63 in the naturalized scenario to 0.68 in the baseline operation scenario, with 8% increase in evaporation loss. Concurrently, the annual streamflow from the baseline operation scenario ($Q_{sim\_base}$) increased with respect to the annual $Q_{sim\_nat}$, leading to a greater $\Delta S_{sim\_base}$ than $\Delta S_{sim\_nat}$. Table 1 (the last two rows) also shows the water balance components in the baseline operation scenario at the reservoir scale compared to the measurements of reservoir outflow and storage change. For the Sirikit reservoir, the annual $Q_{sim\_base}$ tends to be smaller than the annual $Q_{obs}$. The difference between the $\Delta S_{sim\_base}$ and $\Delta S_{obs}$ is also large since they were both computed by closing the water balance.

**Table 1**
Yearly averages of water balance components [mm year$^{-1}$] obtained from the naturalized scenario (sim_nat), baseline operation scenario (sim_base) and observations (obs) for the study catchments and individual reservoirs. The components comprise MSWEP V2 precipitation (*P*), eartH2Observe potential evapotranspiration (*PET*), simulated actual evapotranspiration (*AET*), simulated inflow (*I*), simulated and observed streamflows (*Q*), and simulated and observed changes in water storage (*ΔS*). For the observations, the *ΔS* values of the four catchments were calculated based on the MSWEP V2 *P* and the simulated *AET* as residual of the water balance. For the water balance at the reservoir scale (the last two rows), *ΔS* represents the reservoir storage change. The simulated *ΔS* data of the reservoirs were obtained from the ROM and the observed *ΔS* data were available from RID observations. Note that the *P* and *PET* values in this table were calculated in the period of available observed *Q* for each catchment.

| Catchment/reservoir | P | I | PET | sim_nat | | | sim_base | | | obs | | Year |
|---|---|---|---|---|---|---|---|---|---|---|---|---|
| | | | | AET | Q | ΔS | AET | Q | ΔS | Q | ΔS | |
| Nan_natural | 1261 | 0 | 1031 | 725 | 540 | − 5 | | | | 766 | − 230 | 1994–2013 |
| Yom_natural | 1114 | 0 | 1082 | 741 | 364 | 10 | | | | 386 | − 13 | 1996–2013 |
| Sirikit catchment | 1114 | 2279 | 1190 | 750 | 2645 | − 2 | 810 | 2685 | − 102 | 2814 | − 231 | 1989–1997, 2003–2013 |
| Bhumibol catchment | 942 | 835 | 1093 | 654 | 1123 | − 1 | 669 | 1102 | 6 | 780 | 328 | 1989–2013 |
| Sirikit reservoir | 1202 | 16,703 | 1205 | | | | 1203 | 17,193 | − 488 | 18,019 | − 610 | 1989–1997, 2003–2013 |
| Bhumibol reservoir | 889 | 25,964 | 1126 | | | | 1122 | 25,503 | 229 | 18,050 | − 337 | 1989–2013 |

The simulated water balance in the baseline operation scenario of the Bhumibol catchment, on the other hand, is similar to its water balance in the naturalized scenario (Table 1). This catchment is also located midstream and receives inflows from upstream (see its location in Fig. 1). Due to the prompt surcharge releases by the ROM, the $Q_{\text{sim\_base}}$ behaved like the $Q_{\text{sim\_nat}}$ in very wet periods, as also evident in Fig. 2(D). As a result, *AET/PET* ratios in the naturalized scenario (0.60) and baseline operation scenario (0.61) were almost the same, with only 2% increase in evaporation loss by reservoir operation. The annual $Q_{\text{sim\_base}}$ for the Bhumibol reservoir was much higher than its annual $Q_{\text{obs}}$, leading to the large gap between the $\Delta S_{\text{sim\_base}}$ and $\Delta S_{\text{obs}}$.

Focusing on the Sirikit catchment, the dissimilarity in magnitude and timing of its cumulative $Q$ time series between the naturalized and baseline operation scenarios further clarifies the reservoir effects on the catchment water balance (Fig. 3). In the naturalized
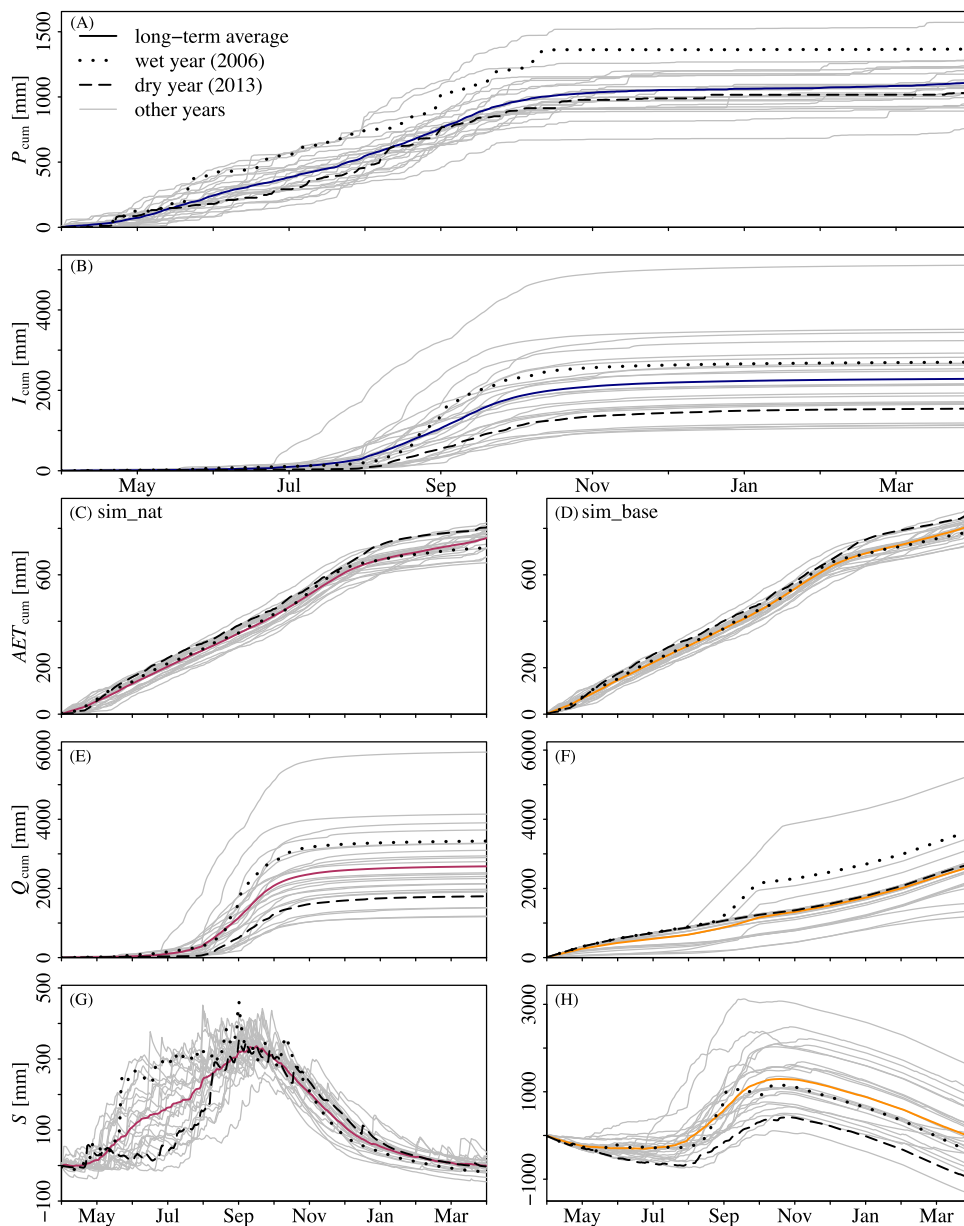


**Fig. 3.** Cumulative daily water balance components for the Sirikit catchment in the naturalized and baseline operation scenarios. The components comprise cumulative precipitation ($P_{\text{cum}}$; panel (A)), inflow ($I_{\text{cum}}$; panel (B)), actual evapotranspiration ($AET_{\text{cum}}$; panel (C) and (D)), streamflow ($Q_{\text{cum}}$; panel (E) and (F)) and storage with respect to the start of the year ($S$; panel (G) and (H)). Data from the years 1989 to 2013 are shown in gray lines. The long-term averages of $P_{\text{cum}}$ and $I_{\text{cum}}$ remain the same between the naturalized and baseline operation scenarios and are shown in blue lines. The long-term average values of the other three components are shown in red lines for the naturalized scenario (sim_nat; left panels) and orange lines for the baseline operation scenario (sim_base; right panels). The black dotted lines represent the selected wet year (2006), while the black dashed lines represent the selected dry (2013) year.

scenario, the long-term mean cumulative $Q_{sim\_nat}$ (red line in Fig. 3(E)) increased dramatically from July to October, consistently with the long-term mean cumulative $P$ and $I$ (blue lines in Fig. 3(A) and (B)). The cumulative $Q_{sim\_nat}$ was significantly higher in the wet year (2006; dotted line) than in the dry year (2013; dashed line). On the contrary, the long-term mean cumulative $Q_{sim\_base}$ (orange line in Fig. 3(F)) increased more gradually over the period of one year. Exceptions are found for 2006 and other wet years, when the cumulative $Q_{sim\_base}$ surged in the rainy season due to the ROM surcharge releases, as also evident in Fig. 2(C). Notably, the cumulative $Q_{sim\_base}$ in 2013 is comparable to the long-term average, despite the lower $P$ and $I$.

Fig. 3 also illustrates the different patterns of the Sirikit catchment storage in the naturalized and baseline operation scenarios, here called $S_{sim\_nat}$ and $S_{sim\_base}$ (because the cumulative value of the catchment storage changes is a catchment storage with respect to the initial condition). The long-term mean $S_{sim\_nat}$ (red line in Fig. 3(G)) increased during the first half of the year, peaking in mid-September (330 mm) before dropping to around zero by the end of the year. In 2006, the $S_{sim\_nat}$ rose strikingly since the beginning of the rainy season in response to storm water. In 2013, on the other hand, it remained small until July as monsoons arrived later than usual. In contrast, the long-term mean $S_{sim\_base}$ (orange line in Fig. 3(H)) slightly decreased from the start of the year and remained negative until August. After that, it rose to a peak in mid-October (1285 mm). In the latter half of the year, the $\Delta S_{sim\_base}$ volume steadily declined. A smaller negative $\Delta S_{sim\_base}$ value was found at the end of 2013 than 2006.

### 5.3. Effects of reservoir operation on the daily flow regime

The daily $Q_{sim\_nat}$ time series of the Sirikit catchment deviated significantly from the $Q_{sim\_base}$ and $Q_{obs}$ time series, as visible in Fig. 2(C). The $Q_{sim\_nat}$ time series presented a strong seasonal variation, with very low flows in the dry season and steep rising limbs and high peak flows in the rainy season. Meanwhile, the $Q_{sim\_base}$ and $Q_{obs}$ time series were smoother, with higher flows in the dry season and diminished peak flows in the rainy season. The $Q_{sim\_base}$ time series, however, had a short period with high peak flows from the reservoir surcharge releases by the ROM. The poor fits between the $Q_{sim\_nat}$ and $Q_{obs}$ for the Sirikit catchment reflect the effect of reservoir operation on daily streamflow. In addition, the difference between the $Q_{sim\_base}$ and $Q_{obs}$ indicates the effect of real-time operation with decision making on top of the generalized operation rules.

The daily FDCs and flow signatures of the Sirikit catchment are different among the naturalized scenario (FDC$_{sim\_nat}$), baseline operation scenario (FDC$_{sim\_base}$), and observation (FDC$_{obs}$), as demonstrated in Fig. 4 and Table 2. Overall, the FDC$_{sim\_nat}$ is steeper than the FDC$_{sim\_base}$ and FDC$_{obs}$, as indicated by the greater Slope$_{FDC}$ values. The flattening of the FDC$_{sim\_base}$ and FDC$_{obs}$ is the result of increasing mean flow and low flow, and reducing high flow. The FDC$_{sim\_base}$ shows less variability, with lower Slope$_{FDC}$, compared to the FDC$_{obs}$ due to lower high flows and higher low flows. In addition, the FDC$_{sim\_base}$ differed more from the FDC$_{obs}$ in the dry year (2013) than in the wet year (2006) as the $Q_{sim\_base}$ maintained low flows at a higher level. Notably, the $Q_{sim\_nat}$ and $Q_{sim\_base}$ were perennial throughout the study period, whereas the $Q_{obs}$ ceased for 4% of the time during the years 1989–1997. The flow signatures also differ between the years 1989–1997 and the years 2003–2013, with increased median, high and low flows in the latter period in all scenarios.

In accordance with the steep slope of the FDC$_{sim\_nat}$, the $Q_{sim\_nat}$ for the Sirikit catchment received only a small contribution from baseflow (low BFI) and was very flashy (high FI), as illustrated in Table 2 and Fig. 5. The BFI$_{sim\_nat}$ = 0.62 and FI$_{sim\_nat}$ = 0.22 in the years 1989–1997 express that the $Q_{sim\_nat}$ had a baseflow contribution of 62% and an average day-to-day fluctuation of 22%. Similar
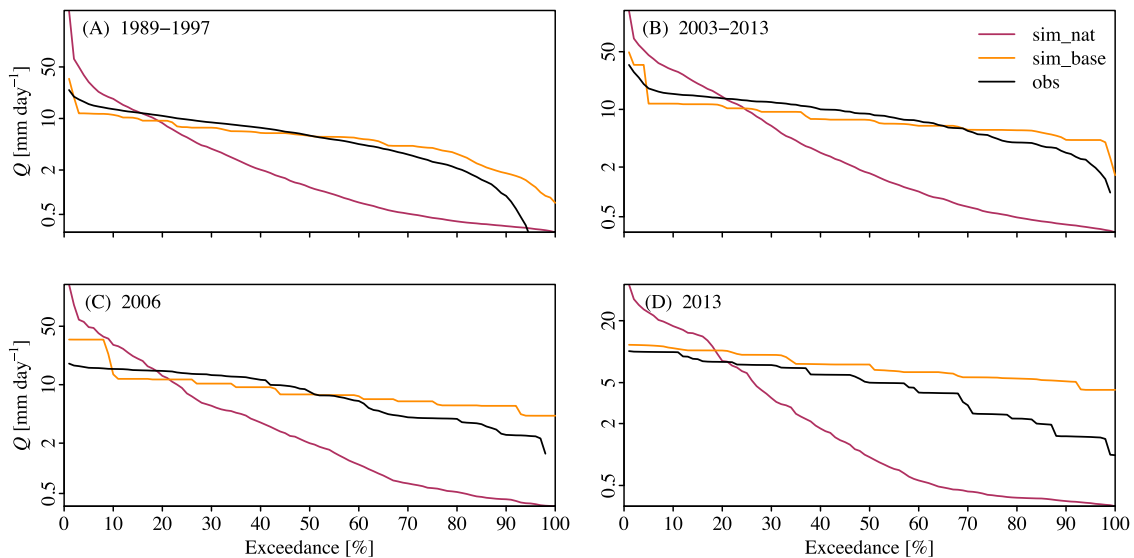


**Fig. 4.** Simulated and observed daily flow-duration curves of the Sirikit catchment during 1989–1997 (A), 2003–2013 (B), the wet year 2006 (C) and the dry year 2013 (D). The streamflows are shown on a logarithmic scale. The streamflow in the naturalized scenario (sim_nat) is shown in red lines, the baseline operation scenario (sim_base) in orange lines and observation (obs) in black lines.

**Table 2**
Signatures of daily streamflow from the simulations and observation for the Sirikit catchment. High flows are defined as the flows that are exceeded 10% of the time, and low flows as being exceeded 90% of the time.

| Signature | Years 1989–1997 | | | Years 2003–2013 | | | Year 2006 (wet) | | | Year 2013 (dry) | | |
|---|---|---|---|---|---|---|---|---|---|---|---|---|
| | sim_nat | sim_base | obs | sim_nat | sim_base | obs | sim_nat | sim_base | obs | sim_nat | sim_base | obs |
| Median flow [mm day$^{-1}$] | 1.17 | 5.82 | 5.86 | 1.68 | 7.44 | 8.82 | 2.00 | 7.65 | 8.23 | 0.94 | 7.5 | 5.00 |
| High flow [mm day$^{-1}$] | 18.46 | 11.20 | 13.38 | 29.88 | 11.74 | 15.40 | 29.97 | 13.29 | 15.43 | 17.73 | 10.82 | 9.91 |
| Low flow [mm day$^{-1}$] | 0.35 | 1.81 | 0.89 | 0.40 | 4.27 | 2.98 | 0.43 | 5.59 | 2.51 | 0.35 | 5.15 | 1.51 |
| Slope$_{FDC}$ [–] | 5.22 | 1.46 | 2.43 | 5.46 | 1.18 | 2.02 | 5.64 | 1.30 | 3.17 | 5.64 | 1.09 | 1.73 |
| BFI [–] | 0.62 | 0.95 | 0.40 | 0.64 | 0.95 | 0.81 | 0.73 | 0.87 | 0.73 | 0.68 | 0.98 | 0.89 |
| FI [–] | 0.22 | 0.02 | 0.28 | 0.18 | 0.02 | 0.08 | 0.20 | 0.04 | 0.10 | 0.18 | 0.01 | 0.04 |

index values are found for the years 2003–2013. The $Q_{sim\_base}$, on the contrary, presented significantly higher BFI and lower FI values, in line with the flatter FDC curves in both the 1989–1997 and 2003–2013 periods. Note that in the baseline operation scenario and observation, the BFI is no longer representing slowly emptying aquifers but emptying reservoirs. Although the $FDC_{sim\_base}$ and $FDC_{obs}$ show relatively similar shapes (Fig. 4), the $Q_{obs}$ was more flashy and had a lower baseflow contribution than the $Q_{sim\_base}$ (Fig. 5). Especially in the years 1989–1997, the $Q_{obs}$ was even more flashy, with a lower baseflow contribution than the $Q_{sim\_nat}$ (Table 2). The $BFI_{obs}$ increased and the $FI_{obs}$ reduced in the years 2003–2013. All scenarios indicate that the streamflow was slightly more flashy in the wet years than in the dry years.

### 5.4. Effects of reservoir operation on extreme flows

The annual maximum daily flows (*AMAX*) for the Sirikit catchment were significantly higher in the naturalized scenario ($AMAX_{sim\_nat}$) than in the baseline operation scenario ($AMAX_{sim\_base}$) and observation ($AMAX_{obs}$), as illustrated in Fig. 6(A). The $AMAX_{sim\_nat}$ showed notable inter-annual variability, whereas the $AMAX_{sim\_base}$ and $AMAX_{obs}$ were more stable throughout the 25-year period. The long-term mean of *AMAX* decreased from the naturalized scenario (92 mm day$^{-1}$) by 84% to the baseline operation scenario and the observation (15 mm day$^{-1}$). The highest *AMAX* volume in the naturalized scenario (292 mm day$^{-1}$ in 1989) was significantly greater than in the baseline operation scenario (49 mm day$^{-1}$ in 2011) and the observation (35 mm day$^{-1}$ in 2011). The differences in *AMAX* among the two simulation scenarios and the observation were larger in the wet years than in the dry years.

The annual daily minimum flows (*AMIN*) for the Sirikit catchment were significantly lower in the naturalized scenario ($AMIN_{sim\_nat}$) than in the baseline operation scenario ($AMIN_{sim\_base}$), as demonstrated in Fig. 6(B). The long-term mean of *AMIN* increased from the naturalized scenario (0.3 mm day$^{-1}$) by 1567% to the baseline operation scenario (5 mm day$^{-1}$) and by 507% to the observation (2 mm day$^{-1}$). The $AMIN_{sim\_nat}$ remained less than 1 mm day$^{-1}$, but the river was not ephemeral. The $AMIN_{sim\_base}$ remained lower than 7 mm day$^{-1}$. Interestingly, the observation ($AMIN_{obs}$) showed more variability, with an evident increasing trend from the years 1989–1997 (less than 1 mm day$^{-1}$) to the years 2003–2013 (1–5 mm day$^{-1}$), in line with the BFI in Fig. 5(A). Note that the $AMIN_{obs}$ reached zero six times during the 1989–1997 period.

The return periods of *AMAX* for the Sirikit catchment indicate that annual flood peaks occurred most frequently and with the highest magnitudes in the naturalized scenario (Fig. 7(A)). The 5-year-return-period flood was significantly reduced from the naturalized scenario (135 mm day$^{-1}$) by approximately 84% to the baseline operation scenario (22 mm day$^{-1}$) and observation (20 mm day$^{-1}$). The $AMAX_{sim\_nat}$ with the up-to-5-year return periods tend to take place in August and September (Fig. 7(B)). On the other hand, the $AMAX_{sim\_base}$ and $AMAX_{obs}$ with the up-to-5-year return periods tend to take place in May, which is the transition period from the dry season to the rainy season and thus may not cause as severe flooding as those occurred in August–October.

The return periods of *AMIN* for the Sirikit catchment indicate that annual minimum flows occurred most frequently and severely in the naturalized scenario (Fig. 7(C)). The 5-year-return-period minimum flow increased from the naturalized scenario (0.3 mm day$^{-1}$) by 1233% to the baseline operation scenario (4 mm day$^{-1}$) and by 100% to the observation (0.6 mm day$^{-1}$). Fig. 7(D) shows that the $AMIN_{sim\_nat}$ with the up-to-5-year return periods tend to occur in the end of the dry season (March–April). The $AMIN_{sim\_base}$ and $AMIN_{obs}$ with the up-to-5-year return periods, on the other hand, tend to occur in the beginning of the dry season (November).

### 5.5. Effects of extreme weather on extreme flows

Fig. 8 illustrates the relationship between extreme flows, including *AMAX* and *AMIN*, and cumulative amounts of effective inflow ($P + I - AET$) in one day and 30 days prior to the extreme flow incidents. The cumulative effective inflows had an influence on the
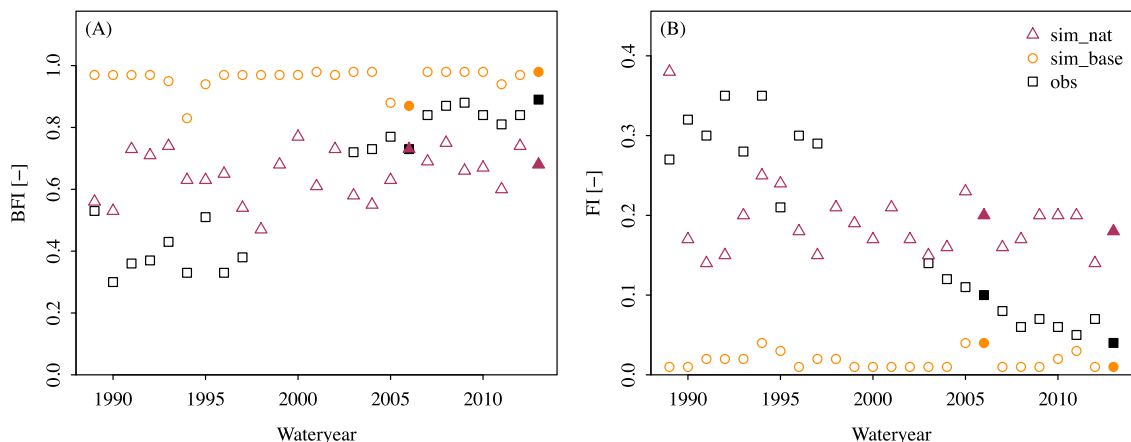


**Fig. 5.** Yearly base flow index (A) and flashiness index (B) of the simulated and observed daily streamflows for the Sirikit catchment. The index values in the naturalized scenario (sim_nat) are shown in red triangles, the baseline operation scenario (sim_base) in orange circles and the observation (obs) in black squares. The filled symbols represent the index values in the wet year (2006) and dry year (2013).
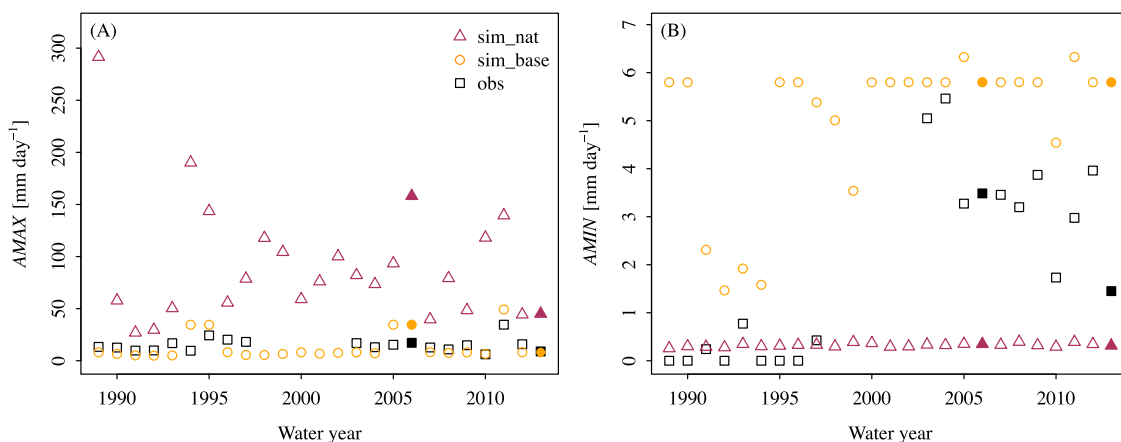
**Fig. 6.** Annual maximum daily flows (A) and annual minimum daily flows (B) from the simulations and observation for the Sirikit catchment. The values in the naturalized scenario (sim_nat) are shown in red triangles, the baseline operation scenario (sim_base) in orange circles and the observation (obs) in black squares. The filled symbols represent the values in the wet year (2006) and dry year (2013). Note that the annual maximum flows were computed in the rainy season, while the annual minimum flows were computed in the dry season to exclude the flows that did not cause flood or drought issues.
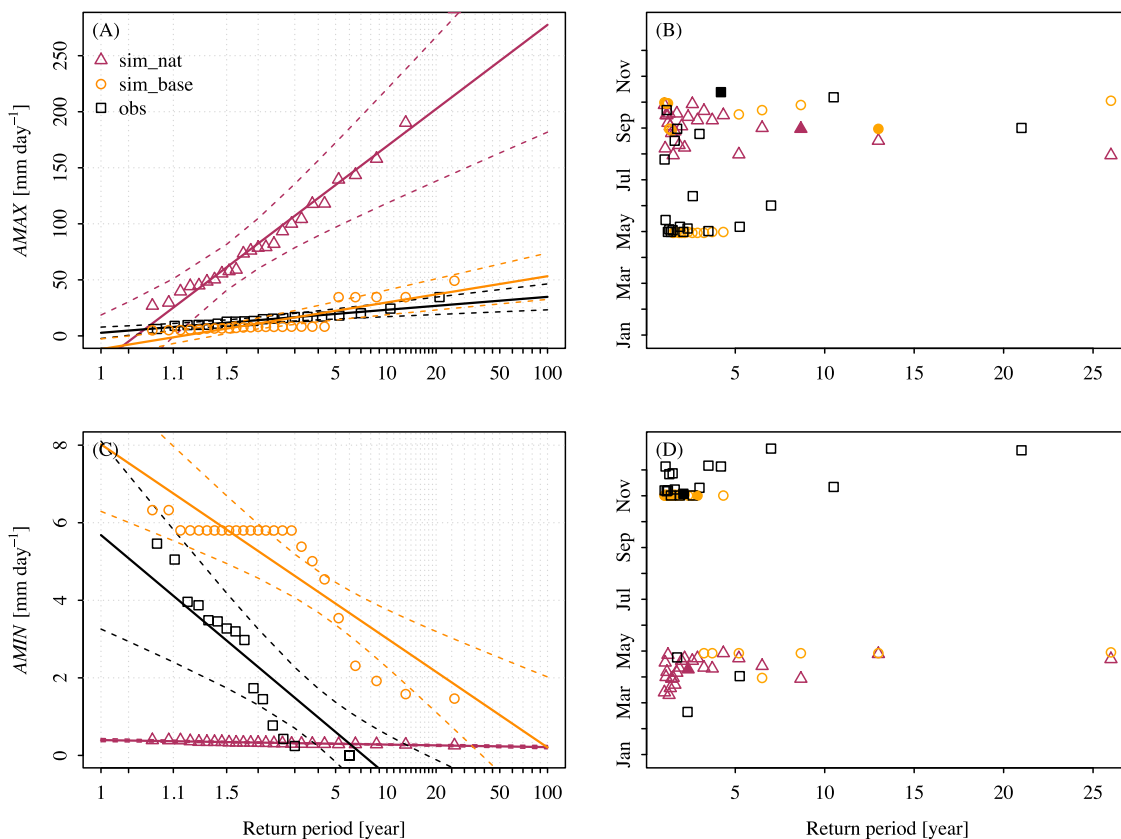


**Fig. 7.** Return periods of the simulated and observed extreme flows, including the annual maximum daily flows (*AMAX*; panels A,B) and annual minimum daily flows (*AMIN*; panels C,D) for the Sirikit catchment based on the Gumbel distribution. Figures A and C show the relation between the magnitude and frequency of the extreme flows. The symbols represent actual values of extreme flows, solid lines represent the probability distribution and dashed lines represent the 95% confidence interval. The values in the naturalized scenario (sim_nat) are shown in red, the baseline operation scenario (sim_base) in orange and the observation (obs) in black. Figures B and D show the relation between the frequency and timing of the extreme flows. The filled symbols represent the values in the wet year (2006) and dry year (2013). Note that the annual maximum flows were computed from the rainy season, while the annual minimum flows were computed from the dry season in order to exclude the flows that did not cause flood or drought issues.

*AMAX*, especially in the naturalized scenario (Fig. 8(A) and (C)). The $AMAX_{sim\_nat}$ has the highest correlation to the one-day effective inflow ($R^2 = 0.92$), the $AMAX_{sim\_base}$ to the 30-day effective inflow ($R^2 = 0.45$), and the $AMAX_{obs}$ to the 30-day effective inflow ($R^2 = 0.21$). On the other hand, there is no clear relation between *AMIN* and effective inflow in any scenario (Fig. 8(B) and (D)).

## 6. Discussion

### 6.1. Effects of reservoir operations on the water balance

The water balance of the Sirikit and Bhumibol catchments changed significantly from the naturalized scenario to the baseline operation scenario in terms of magnitude and timing. The higher annual *AET* in the baseline operation scenario resulted from the direct evaporation from the reservoir water surface and streamflow (Table 1). The corresponding trends between *P* and *I*, and the rapid $Q_{sim\_nat}$ (visible as sharp increase of its cumulative) indicate the natural rainfall-runoff process with a quick catchment response (Fig. 3). On the other hand, the steady $Q_{sim\_base}$ (visible as gradual increase of its cumulative) and the large annual $\Delta S_{sim\_base}$ values imply that the reservoir operations markedly altered the natural rainfall-runoff process with a longer residence time of water. The effects of the reservoir operation on the water balance were apparent in dry years as the reservoirs tried to fulfill the target downstream water demand with stored water from the previous rainy season, although this led to a very low reservoir storage at the end of the year.

It should be kept in mind that the aforementioned effects refer to the baseline reservoir operation with the generalized operation rules (by the ROM), which are different from the real-time reservoir operation (observations). Since only the observed reservoir storage and outflow are available, we could not thoroughly analyze the effects of the real-time operation on the water balance. However, it is obvious that the real-time operation is unique and much more flexible for each reservoir due to the circumstance-specific judgments by dam operators, affecting the water balance to another extent. This was reflected in the higher annual streamflow for the Sirikit catchment but lower annual streamflow for the Bhumibol catchment compared to their naturalized flows (Table 1).
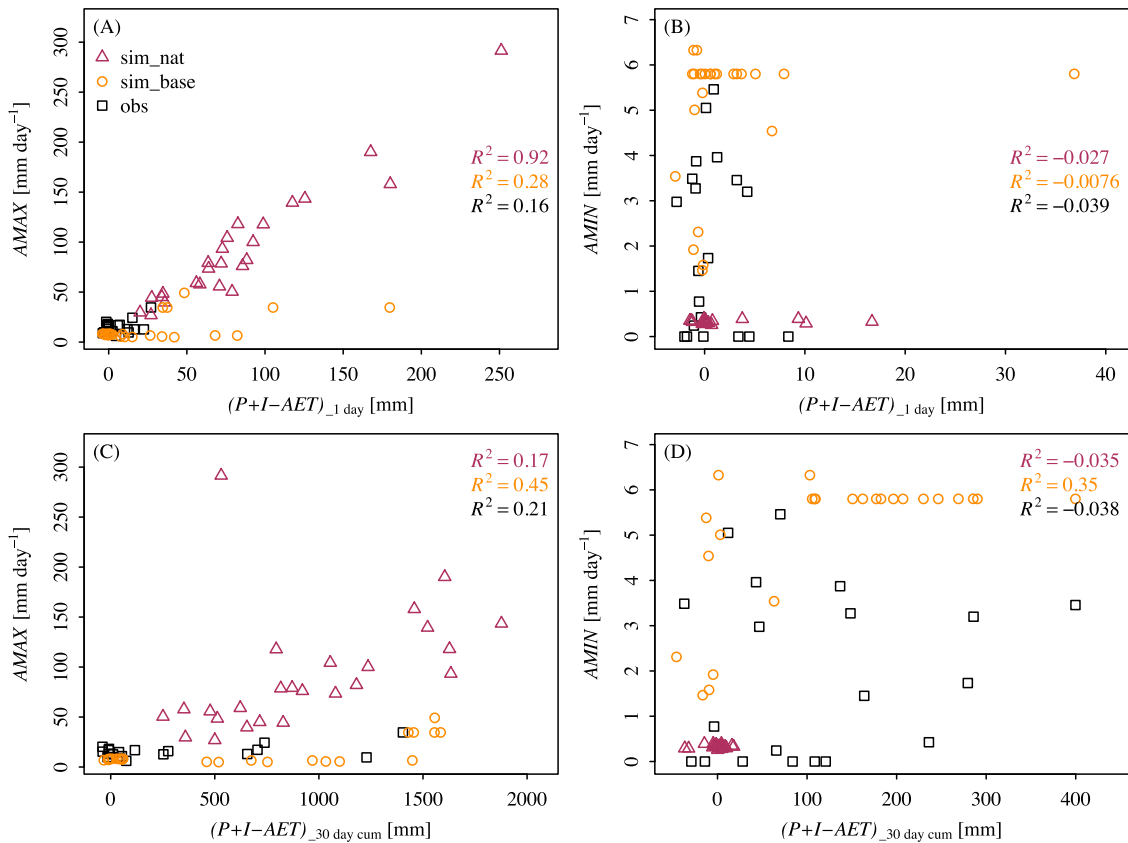


**Fig. 8.** Relationship between cumulative effective inflows and daily extreme flows, including annual maximum daily flows (left panels) and annual minimum daily flows (right panels) from the simulations and observation for the Sirikit catchment. The values in the naturalized scenario (sim_nat) are shown in red triangles, the baseline operation scenario (sim_base) in orange circles and the observation (obs) in black squares. The effective inflows (x axis) is the sum of precipitation (*P*) and inflow (*I*) minus the actual evapotranspiration (*AET*) on the day that an extreme flow occurred (first row) and the cumulative amount 30 days prior to the extreme flow date (second row).

## 6.2. Effects of reservoir operations on the daily flow regime

Major alterations by the reservoir operations were the flatter FDC and more smooth flow regime due to increasing daily median flows ($Q_{50}$) and daily low flows ($Q_{90}$), and decreasing daily high flows ($Q_{10}$) compared to the naturalized flow (Fig. 4 and Table 2). The reservoir operations completely inverted the seasonality of the naturalized flow regime, with significantly higher daily streamflow in the dry season and lower daily streamflow in the rainy season (Fig. 2(C) and (D)). Hanasaki et al. (2006) and Yassin et al. (2019) also reported similar results for the Sirikit and Bhumibol reservoirs. The high reservoir outflows in the dry season were mainly to compensate environmental flows, including downstream irrigation supply and hydropower generation. At the same time, the draw-down of reservoir storage provided space to restore water in the next rainy season. Meanwhile, the low reservoir outflows in the rainy season were to prevent overflows in the downstream floodplains. Changes in the daily flow regime were more complicated with the real-time operation than with the baseline operation. A good example is when the real-time operation slowly released the surcharge water or paused the daily release to prevent or moderate flooding downstream (Fig. 2(C) and (D)).

Since water in the upper GCPR basin comes from seasonal precipitation, the naturalized flow was very variable (low BFI and high FI; Fig. 5), causing the basin to be at risk of both flash floods and intensive dry periods. On the other hand, the regulated flow with the baseline operation had a high and stable baseflow contribution from the reservoir storage (high BFI and low FI). This indicates that the daily streamflow was not flashy and enabled to sustain the minimum water demands in the period of low or absent precipitation. The real-time operation, however, failed to overcome these problems during 1989–1997, but significantly improved with more daily baseflow contribution and less daily flashiness in 2003–2013. More experiences of dam operators gained over time may have been relevant for this improvement.

## 6.3. Effects of reservoir operations on extreme flows

Both baseline and real-time reservoir operations substantially reduced the magnitude and frequency of the annual flood peaks (annual maximum daily flows), although the extent of the effects varied between years. Most of the naturalized flood peaks in the rainy season were absorbed by the reservoirs, as visible in Fig. 2(C) and 2(D). The magnitudes of annual flood peaks (Fig. 6(A)) and the 5-year-return-period flood (Fig. 7(A)) were significantly diminished by both baseline and real-time operations, especially in wet years. This included the 2011 catastrophic flooding that affected the entire GCPR basin. Interestingly, timing of the annual flood peak incidents shifted and became more variable with the real-time operation (Fig. 7(B)). It should be noted that the annual flood peaks that occurred in May are unlikely to cause flooding as it is the beginning of the rainy season after a prolonged dry period. The naturalized annual flood peaks and the annual flood peaks with the baseline operation usually occurred in August and September. Meanwhile, the real-time operation disrupted this pattern, causing the annual flood peaks to take place from June to October. For this reason, the real-time operation alleviated many historical flood incidents, but at the same time their variable timing can pose a challenge in the reservoir system modeling.

The severity and frequency of the annual minimum flows also markedly declined with the baseline operation (Figs. 6(B) and 7 (C)). However, the real-time operations worsened the annual minimum flows in the years 1989–1997. During this period, the observed annual minimum flows were lower than those in the naturalized scenario and even ceased in some dry seasons, indicating that the real-time operation might trigger some drought events. These drastic minimum flows were eliminated in the years 2003–2013, correspondingly to the BFI improvement. The timing of the annual minimum flows also shifted (Fig. 7(D)). Note that the annual minimum flows occurring in November–December usually do not lead to water shortage as the extensive monsoon period just passed. The naturalized annual minimum flows occurred in March and April, which is the driest period of the years, thus putting the basin at risk of droughts. The real-time operation apparently solved this issue better than the baseline operation, with only three years of the annual minimum flows occurring in the drought-risk period.

## 6.4. Effects of extreme weather on extreme flows

The reservoir operations were the main cause of the inconsistency in the relationship between the effective inflows ($P + I - AET$) and annual flood peaks in the baseline and real-time operation scenarios (Fig. 8). Therefore, based on our results, it is likely that the reservoir operation played a more important role than extreme weather in mitigating or magnifying the extreme flow events in the upper GCPR basin. However, the slightly positive correlation between the effective inflows and annual flood peaks indicates that extreme precipitation events magnified historical flood incidents to some extent, although they were not as severe as those in the naturalized scenario. Similar results were reported by Komori et al. (2012) and Sayama et al. (2015). Unfortunately, it is difficult to completely separate the roles of extreme weather and the reservoir operation.

This study did not explicitly account for effects of climate variability on extreme flows and the Gumbel extreme value analyses (Fig. 7) assumed that there was no trend in annual precipitation. However, we acknowledge the probable changes in monsoon patterns in term of magnitudes, timing and direction over the past decades in SEA and Thailand (e.g., Singhrattna et al., 2005; Loo et al., 2015). The shift in monsoon direction, for example, can result in less reservoir inflow, and concurrently more direct floodwater in the downstream region. These climate factors influence extreme weather events and real-time reservoir operations, which will affect extreme flows.

*6.5. Effects of real-time control on extreme flows*

According to our findings, we deduce that the generalized operation rules (as represented by the baseline operation scenario) alone could not effectively manage the reservoir water resources throughout a year and that decision making and real-time control (as represented by the observation) are necessary for preventing and mitigating extreme flow incidents. There was apparently a change in the real-time operation from the 1989–1997 period to the 2003–2013 period, resulting in the notable improvements in the streamflow signatures (Table 2 and Fig. 5). It highlights the importance of experience in decision making of dam operators gained over time. As a result, we acknowledge that the Gumbel extreme value analyses of the observation should be interpreted with care. With the real-time control, the reservoir could, for instance, release more water in drier years and close the spillway for a while in wetter years to prevent overtopping the downstream floodwater during storm events. For some events in the past, however, the real-time operation was problematic, such as when the reservoir stored too much storm water and had to release surcharge water to prevent dam failures, thus intensifying downstream inundations (Komori et al., 2012). This underlines the need of more effective real-time forecasting and decision-supporting tools in order to provide more sustainable reservoir operations in the future.

## 7. Conclusion and outlook

The upper GCPR basin has been highly regulated by multipurpose reservoirs for over half a century. While the reservoirs support agriculture and hydropower generation, their regulations have modified the natural flows, posing a challenge to water resource management. This study explored the quantitative effects of the major reservoirs, Sirikit and Bhumibol, on the water balance, daily flow regime and extreme flows during the 1989–2013 period. We used the global-data-driven wflow_sbm model to simulate streamflows in the naturalized scenario (without reservoir) and the baseline operation scenario (with generalized operation rules) as described in detail in the companion paper (Wannasin et al., 2021). We analyzed key hydrological signatures in both scenarios and compared these to the observational data, which represent the real-time operation. The main findings are as follows:

1. The reservoir operation disrupted the natural water balance and rainfall-runoff processes in terms of both magnitude and timing, especially with higher evaporation loss.
2. The reservoir operation inverted the natural seasonality of the daily flow regime, with higher flows in the dry season and lower flows in the rainy season. In the long-term, the daily median flows ($Q_{50}$) and low flows ($Q_{90}$) markedly increased, while daily high flows ($Q_{10}$) markedly reduced. The daily baseflow contribution was greater, indicating that streamflow came mostly from the delayed source (reservoirs), and thus that the daily flows became less flashy and more constant throughout a year.
3. The reservoir operation prevented or mitigated many extreme flow incidents in the past. It reduced the magnitude of annual flood peaks and increased the annual minimum flows. Most of the annual minimum flows were also maintained above the naturalized environmental flows, except in some dry seasons during the 1990s. Both annual flood peaks and minimum flows occurred less frequently, but their timing became more variable and thus difficult to predict.
4. Annual flood peaks and minimum flows were more influenced by the real-time reservoir operation than by extreme weather. However, extreme weather does tend to amplify the severity of flooding.
5. The difference between reservoir outflows from the baseline operation (simulation) and from the real-time operation (observation) highlights the importance of decision making and real-time control to optimize reservoir outflows on the daily basis.

The findings on the effects of reservoir operation in the upper GCPR basin can benefit Thailand in the light of sustainable reservoir management under the recent National Water Resource Management Master Plan for the 2019–2037 period. At a larger scale, the insights of the reservoir effects from this basin can be of assistance to dam operators and water managers for both existing and planned reservoirs in SEA and other tropical regions. In the future, the river basins in Thailand and SEA will probably be more intensively regulated by more reservoirs. Such management needs to be carefully planned in all aspects of hydrology, ecology and economic development to optimize water resources and prevent hydrological hazards. More studies on the effects of other reservoirs, considering their different purposes, sizes and locations are encouraged. The future challenge lies in optimizing the real-time operations for a more effective and sustainable operational and strategic water management, especially for floods and droughts under changing climate and rapid economic development.

## Author statement

**C. Wannasin**: Conceptualization, Methodology, Software, Formal analysis, Investigation, Data Curation, Writing – Original Draft, Visualization.
**C.C. Brauer**: Conceptualization, Methodology, Validation, Writing – Review & Editing, Supervision.
**R. Uijlenhoet**: Conceptualization, Methodology, Validation, Writing – Review & Editing, Supervision.
**W.J. van Verseveld**: Software, Resources, Writing – Review & Editing.
**A.H. Weerts**: Conceptualization, Methodology, Software, Validation, Resources, Writing – Review & Editing, Supervision.

## Conflicts of interest

The authors declare that they have no known competing financial interests or personal relationships that could have appeared to

influence the work reported in this paper.

## Declaration of Competing Interest

The authors report no declarations of interest.

## Acknowledgments

## Appendix A. Supplementary data

Supplementary data associated with this article can be found, in the online version, at https://doi.org/10.1016/j.ejrh.2021. 100792.

## References

Apichitchat, S., Jung, K., 2015. Hydrological simulation for impact assessment of Kaeng Sue Ten dam in Thailand. KSCE J. Civil Eng. 19, 2325–2332. https://doi.org/ 10.1007/s12205-015-0322-3.

Arnell, N.W., Gosling, S.N., 2016. The impacts of climate change on river flood risk at the global scale. Clim. Change 134, 387–401. https://doi.org/10.1007/s10584-014-1084-5.

Baker, D.B., Richards, R.P., Loftus, T.T., Kramer, J.W., 2004. A new flashiness index: characteristics and applications to midwestern rivers and streams. J. Am. Water Resour. Assoc. 40, 503–522. https://doi.org/10.1111/j.1752-1688.2004.tb01046.x.

Batalla, R.J., Gomez, C.M., Kondolf, G.M., 2004. Reservoir-induced hydrological changes in the Ebro River basin (NE Spain). J. Hydrol. 290, 117–136. https://doi.org/10.1016/j.jhydrol.2003.12.002.

Beck, H.E., Wood, E.F., Pan, M., Fisher, C.K., Miralles, D.G., Van Dijk, A.I., McVicar, T.R., Adler, R.F., 2019. MSWEP V2 global 3-hourly 0.1° precipitation: methodology and quantitative assessment. Bull. Am. Meteorol. Soc. 100, 473–500. https://doi.org/10.1175/BAMS-D-17-0138.1.

Bontemps, S., Defourny, P., Van Bogaert, E., Arino, O., Kalogirou, V., Perez, J.R., 2011. GLOBCOVER 2009-Products Description and Validation Report. The European Space Agency GlobCover Portal (last accessed on 15/07/2020). http://due.esrin.esa.int/page_globcover.php.

Brakensiek, D., Rawls, W., Stephenson, G., 1984. Modifying SCS Hydrologic Soil Groups and Curve Numbers for Rangeland Soils. Am. Soc. Agri. Eng.

Canuto, N., Ramos, T.B., Oliveira, A.R., Simionesei, L., Basso, M., Neves, R., 2019. Influence of reservoir management on Guadiana streamflow regime. J. Hydrol.: Reg. Stud. 25, 100628. https://doi.org/10.1016/j.ejrh.2019.100628.

Di Baldassarre, G., Wanders, N., AghaKouchak, A., Kuil, L., Rangecroft, S., Veldkamp, T.I., Garcia, M., van Oel, P.R., Breinl, K., Van Loon, A.F., 2018. Water shortages worsened by reservoir effects. Nat. Sustain. 1, 617–622. https://doi.org/10.1038/s41893-018-0159-0.

Durrans, S.R., 1988. 18. Total Probability Methods for Problems in Flood Frequency Estimation. International Conference on Statistical and Bayesian Methods in Hydrological Sciences in honor of Professor Jacques Bernier, Paris, Paris, France, pp. 299–326.

Gai, L., Nunes, J.P., Baartman, J.E., Zhang, H., Wang, F., de Roo, A., Ritsema, C.J., Geissen, V., 2019. Assessing the impact of human interventions on floods and low flows in the Wei River Basin in China using the LISFLOOD model. Sci. Total Environ. 653, 1077–1094. https://doi.org/10.1016/j.scitotenv.2018.10.379.

Gale, E.L., Saunders, M.A., 2013. The 2011 Thailand flood: climate causes and return periods. Weather 68, 233–237. https://doi.org/10.1002/wea.2133.

Gebremicael, T., Mohamed, Y., Van der Zaag, P., 2019. Attributing the hydrological impact of different land use types and their long-term dynamics through combining parsimonious hydrological modelling, alteration analysis and PLSR analysis. Sci. Total Environ. 660, 1155–1167. https://doi.org/10.1016/j.scitotenv.2019.01.085.

Giardino, A., Schrijvershof, R., Nederhoff, C., De Vroeg, H., Brière, C., Tonnon, P.K., Caires, S., Walstra, D., Sosa, J., Van Verseveld, W., et al., 2018. A quantitative assessment of human interventions and climate change on the West African sediment budget. Ocean Coast. Manag. 156, 249–265. https://doi.org/10.1016/j.ocecoaman.2017.11.008.

Graf, W.L., 2006. Downstream hydrologic and geomorphic effects of large dams on American rivers. Geomorphology 79, 336–360. https://doi.org/10.1016/j.geomorph.2006.06.022.

Gustard, A., Bullock, A., Dixon, J., 1992. Low Flow Estimation in the United Kingdom. Institute of Hydrology, pp. 20–25.

Hanasaki, N., Kanae, S., Oki, T., 2006. A reservoir operation scheme for global river routing models. J. Hydrol. 327, 22–41. https://doi.org/10.1016/j.jhydrol.2005.11.011.

Hanasaki, N., Saito, Y., Chaiyasaen, C., Champathong, A., Ekkawatpanit, C., Saphaokham, S., Sukhapunnaphan, T., Sumdin, S., Thongduang, J., 2014. A quasi-real-time hydrological simulation of the Chao Phraya River using meteorological data from the Thai meteorological department automatic weather stations. Hydrol. Res. Lett. 8, 9–14. https://doi.org/10.3178/hrl.8.9.

Hassaballah, K., Mohamed, Y., Uhlenbrook, S., Biro, K., 2017. Analysis of streamflow response to land use and land cover changes using satellite data and hydrological modelling: case study of Dinder and Rahad tributaries of the Blue Nile (Ethiopia-Sudan). Hydrol. Earth Syst. Sci. 21, 5217. https://doi.org/10.5194/hess-21-5217-2017.

He, X., Wada, Y., Wanders, N., Sheffield, J., 2017. Intensification of hydrological drought in California by human water management. Geophys. Res. Lett. 44, 1777–1785. https://doi.org/10.1002/2016GL071665.

Hengl, T., de Jesus, J.M., Heuvelink, G.B., Gonzalez, M.R., Kilibarda, M., Blagotić, A., Shangguan, W., Wright, M.N., Geng, X., Bauer-Marschallinger, B., et al., 2017. SoilGrids250m: global gridded soil information based on machine learning. PLOS ONE 12. https://doi.org/10.1371/journal.pone.0169748.

Hisdal, H., Tallaksen, L.M., Clausen, B., Peters, E., Gustard, A., Van Lanen, H., 2004. Hydrological drought characteristics. Dev. Water Sci. 48, 139–198.

Imhoff, R., van Verseveld, W., van Osnabrugge, B., Weerts, A., 2020. Scaling point-scale (pedo) transfer functions to seamless large-domain parameter estimates for high-resolution distributed hydrologic modeling: an example for the Rhine river. Water Resour. Res. 56 https://doi.org/10.1029/2019WR026807.

Jamrussri, S., Toda, Y., 2017. Simulating past severe flood events to evaluate the effectiveness of nonstructural flood countermeasures in the upper Chao Phraya River Basin, Thailand. J. Hydrol.: Reg. Stud. 10, 82–94. https://doi.org/10.1016/j.ejrh.2017.02.001.

Jarvis, A., Reuter, H.I., Nelson, A., Guevara, E., 2008. Hole-Filled Seamless SRTM Data V4. International Centre for Tropical Agriculture (CIAT) (last accessed on 15/07/2020). http://srtm.csi.cgiar.org.

Kampf, S.K., Burges, S.J., 2010. Quantifying the water balance in a planar hillslope plot: effects of measurement errors on flow prediction. J. Hydrol. 380, 191–202. https://doi.org/10.1016/j.jhydrol.2009.10.036.

Kinouchi, T., Yamamoto, G., Komsai, A., Liengcharernsit, W., 2018. Quantification of seasonal precipitation over the upper Chao Phraya River Basin in the past fifty years based on monsoon and El Niño/Southern oscillation related climate indices. Water 10, 800. https://doi.org/10.3390/w10060800.

Komori, D., Mateo, C.M., Saya, A., Nakamura, S., Kiguchi, M., Klinkhachorn, P., Sukhapunnaphan, T., Champathong, A., Takeya, K., et al., 2013. Application of the probability evaluation for the seasonal reservoir operation on flood mitigation and water supply in the Chao Phraya River watershed, Thailand. J. Disaster Res. 8, 432–446. https://doi.org/10.20965/jdr.2013.p0432.

Komori, D., Nakamura, S., Kiguchi, M., Nishijima, A., Yamazaki, D., Suzuki, S., Kawasaki, A., Oki, K., Oki, T., 2012. Characteristics of the 2011 Chao Phraya River flood in central Thailand. Hydrol. Res. Lett. 6, 41–46. https://doi.org/10.3178/hrl.6.41.

Langat, P.K., Kumar, L., Koech, R., 2019. Identification of the most suitable probability distribution models for maximum, minimum, and mean streamflow. Water 11, 734. https://doi.org/10.3390/w11040734.

Lee, J., Heo, J.H., Lee, J., Kim, N., 2017. Assessment of flood frequency alteration by dam construction via SWAT simulation. Water 9, 264. https://doi.org/10.3390/w9040264.

Li, D., Long, D., Zhao, J., Lu, H., Hong, Y., 2017. Observed changes in flow regimes in the Mekong River basin. J. Hydrol. 551, 217–232. https://doi.org/10.1016/j.jhydrol.2017.05.061.

Loo, Y.Y., Billa, L., Singh, A., 2015. Effect of climate change on seasonal monsoon in Asia and its impact on the variability of monsoon rainfall in Southeast Asia. Geosci. Front. 6, 817–823. https://doi.org/10.1016/j.gsf.2014.02.009.

López López, P., 2018. Application of Global Hydrological Datasets for River Basin Modelling. Utrecht University, Utrecht, the Netherlands, pp. 1–214. Doctoral dissertation.

López López, P., Wanders, N., Schellekens, J., Renzullo, L.J., Sutanudjaja, E., Bierkens, M.F., 2016. Improved large-scale hydrological modelling through the assimilation of streamflow and downscaled satellite soil moisture observations. Hydrol. Earth Syst. Sci. 20, 3059–3076. https://doi.org/10.5194/hess-20-3059-2016.

Matalas, N.C., 1963. Probability Distribution of Low Flows. US Government Printing Office, D.C., US, pp. A1–A27.

Mateo, C.M., Hanasaki, N., Komori, D., Tanaka, K., Kiguchi, M., Champathong, A., Sukhapunnaphan, T., Yamazaki, D., Oki, T., 2014. Assessing the impacts of reservoir operation to floodplain inundation by combining hydrological, reservoir management, and hydrodynamic models. Water Resour. Res. 50, 7245–7266. https://doi.org/10.1002/2013WR014845.

Mittal, N., Bhave, A.G., Mishra, A., Singh, R., 2016. Impact of human intervention and climate change on natural flow regime. Water Resour. Manag. 30, 685–699. https://doi.org/10.1007/s11269-015-1185-6.

O'Connor, J.E., Duda, J.J., Grant, G.E., 2015. 1000 dams down and counting. Science 348, 496–497. https://doi.org/10.1126/science.aaa9204.

Poff, N.L., Allan, J.D., Bain, M.B., Karr, J.R., Prestegaard, K.L., Richter, B.D., Sparks, R.E., Stromberg, J.C., 1997. The natural flow regime. BioScience 47, 769–784. https://doi.org/10.2307/1313099.

Sawicz, K., Wagener, T., Sivapalan, M., Troch, P.A., Carrillo, G., 2011. Catchment classification: empirical analysis of hydrologic similarity based on catchment function in the eastern USA. Hydrol. Earth Syst. Sci. 15, 2895–2911. https://doi.org/10.5194/hess-15-2895-2011.

Sayama, T., Tatebe, Y., Iwami, Y., Tanaka, S., 2015. Hydrologic sensitivity of flood runoff and inundation: 2011 Thailand floods in the Chao Phraya River basin. Nat. Hazards Earth Syst. Sci. 15, 1617–1630. https://doi.org/10.5194/nhess-15-1617-2015.

Schellekens, J., Dutra, E., la Torre, A.M.d., Balsamo, G., van Dijk, A., Weiland, F.S., Minvielle, M., Calvet, J.C., Decharme, B., Eisner, S., et al., 2017. A global water resources ensemble of hydrological models: the eartH2Observe Tier-1 dataset. Earth Syst. Sci. Data 9, 389–413. https://doi.org/10.5194/essd-2016-55.

Schellekens, J., Verseveld van, W., Euser, T., Winsemius, H., Thiange, C., Bouaziz, L., et al., 2019. Openstreams/wflow: Unstable-Master (last accessed on 15/07/2020). https://github.com/openstreams/wflow.

Siciliano, G., Urban, F., Kim, S., Lonn, P.D., 2015. Hydropower, social priorities and the rural-urban development divide: the case of large dams in Cambodia. Energy Policy 86, 273–285. https://doi.org/10.1016/j.enpol.2015.07.009.

Singhrattna, N., Rajagopalan, B., Kumar, K.K., Clark, M., 2005. Interannual and interdecadal variability of Thailand summer monsoon season. J. Clim. 18, 1697–1708. https://doi.org/10.1175/JCLI3364.1.

Takeda, M., Laphimsing, A., Putthividhya, A., 2016. Dry season water allocation in the Chao Phraya River basin, Thailand. Int. J. Water Resour. Dev. 32, 321–338. https://doi.org/10.1080/07900627.2015.1055856.

Tebakari, T., Yoshitani, J., Suvanpimol, P., 2012. Impact of large-scale reservoir operation on flow regime in the Chao Phraya River basin, Thailand. Hydrol. Process. 26, 2411–2420. https://doi.org/10.1002/hyp.9345.

Trenberth, K.E., Dai, A., Van Der Schrier, G., Jones, P.D., Barichivich, J., Briffa, K.R., Sheffield, J., 2014. Global warming and changes in drought. Nat. Clim. Change 4, 17–22. https://doi.org/10.1038/nclimate2067.

Urban, F., Siciliano, G., Nordensvard, J., 2018. China's dam-builders: their role in transboundary river management in South-East Asia. Int. J. Water Resour. Dev. 34, 747–770. https://doi.org/10.1080/07900627.2017.1329138.

Van Oldenborgh, G.J., Urk, A., Allen, M., 2012. The absence of a role of climate change in the 2011 thailand floods. Bull. Am. Meteorol. Soc. 93, 1047–1049.

Vertessy, R.A., Elsenbeer, H., 1999. Distributed modeling of storm flow generation in an Amazonian rain forest catchment: effects of model parameterization. Water Resour. Res. 35, 2173–2187. https://doi.org/10.1029/1999WR900051.

Wannasin, C., Brauer, C., Uijlenhoet, R., van Verseveld, W., Weerts, A., 2021. Daily flow simulation in Thailand Part I: Testing a distributed hydrological model with seamless parameter maps based on global data. Hydrol.: Reg. Stud. https://doi.org/10.1016/j.ejrh.2021.100794.

Wichakul, S., Tachikawa, Y., Shiiba, M., Yorozu, K., 2013. Developing a regional distributed hydrological model for water resources assessment and its application to the Chao Phraya River Basin. J. Jpn. Soc. Civil Eng. Ser. B1 (Hydraul. Eng.) 69. https://doi.org/10.2208/jscejhe.69.I_43. I_43-I_48.

Wu, J., Liu, Z., Yao, H., Chen, X., Chen, X., Zheng, Y., He, Y., 2018. Impacts of reservoir operations on multi-scale correlations between hydrological drought and meteorological drought. J. Hydrol. 563, 726–736. https://doi.org/10.1016/j.jhydrol.2018.06.053.

Yassin, F., Razavi, S., Elshamy, M., Davison, B., Sapriza-Azuri, G., Wheater, H., 2019. Representation and improved parameterization of reservoir operation in hydrological and land-surface models. Hydrol. Earth Syst. Sci. 23, 3735–3764. https://doi.org/10.5194/hess-23-3735-2019.

Yusuf, A.A., Francisco, H., 2009. Climate Change Vulnerability Mapping for Southeast Asia. Economy and Environment Program for Southeast Asia, Singapore, pp. 1–26.

Zajac, Z., Revilla-Romero, B., Salamon, P., Burek, P., Hirpa, F.A., Beck, H., 2017. The impact of lake and reservoir parameterization on global streamflow simulation. J. Hydrol. 548, 552–568. https://doi.org/10.1016/j.jhydrol.2017.03.022.

Zarfl, C., Lumsdon, A.E., Berlekamp, J., Tydecks, L., Tockner, K., 2015. A global boom in hydropower dam construction. Aquat. Sci. 77, 161–170. https://doi.org/10.1007/s00027-014-0377-0.

Zenkoji, S., Tebakari, T., Dotani, K., 2019. Rainfall and reservoirs situation under the worst drought recorded in the Upper Chao Phraya River Basin, Thailand. J. Jpn. Soc. Civil Eng. Ser. G (Environ. Res.) 75. https://doi.org/10.2208/jscejer.75.I_115, 75 I_115-I_124.

Zhou, T., Nijssen, B., Gao, H., Lettenmaier, D.P., 2016. The contribution of reservoirs to global land surface water storage variations. J. Hydrometeorol. 17, 309–325. https://doi.org/10.1175/JHM-D-15-0002.1.